FACTA UNIVERSITATIS
Series: **Mechanical Engineering**
https://doi.org/10.22190/FUME240719039H

Original scientific paper

COMPARATIVE ANALYSIS OF THERMAL PERFORMANCE OF TWO BASE LIQUIDS HAVING TRI-HYBRIDIZED NANOMATERIALS IN A VERTICAL CHANNEL UNDER HALL EFFECTS

Jafar Hasnain

Bahria University Islamabad, Pakistan

Abstract. *The use of nanoparticles with enhanced thermal properties has given nanotechnology a prominent place in modern industrial settings. As opposed to oil or water, which serve as base fluids, nanofluids with superior thermal characteristics, such as thermal diffusion, resistive nature, and increased thermal and electrical conductance, are more effective. This research aims to compare the convective heat transfer in hydromagnetic TiO_2-water nanofluid* (*NF*), *TiO_2-SWCNTs-water hybrid nanofluid* (HNF) and *TiO_2-SWCNTs-MWCNTs-water tri-hybrid nanofluid* (*THNF*) *flow in a vertical channel under the influence of hall current. The flow is oscillatory due to the pressure gradient and the velocity slip is considered at the wall. The radiative heat flux is also considered along with the heat source and sink. As a result of using non-dimensional variables, the fundamental equations of the flow problem are recast in a form that is dimension-free. The solution of the dimensionless equations is obtained in the exact form. The effects of involved parameters are illustrated graphically and studied concerning the flow fields, skin friction, and heat transfer rate. The results reveal that the temperature for the tri-hybridized nanofluid is greater than both hybrid and nanofluids. So, three distinct nanoparticle types can be concentrated for improved thermal performance.*

Keywords: *Tri -hybridized nanofluid, Hall effects, Heat source/sink, Beavers and Joseph slip condition*

1. INTRODUCTION

Nanotubes with small structures and dimensions have attracted a lot of researchers to study their properties from a scientific and technological point of view [1]. The unique structure of nanotubes possesses excellent chemical and physical aspects, and these

Received: July 19, 2024 / Accepted September 05, 2024
Corresponding author: Jafar Hasnain
Bahria University, Shangrilla Road, E-8, Islamabad, Pakistan
E-mail: jafar.buic@bahria.edu.pk

properties can be used in manufacturing various industrial products. CNTs with pure carbon polymer chains are nano-sized cylindrical shapes with one (*SWCNT*) or multiple layers (*MWCNTs*) of graphene sheets. CNTs with multiple layers of graphene sheet possess good stability under an argon atmosphere during the thermal phenomenon. It is because a structural transformation for catalytically grown *SWCNTs* was detected for the first time at 1200℃ [2]. Titanium dioxide is significant due to its photocatalytic applications. High photocatalysis properties are obtained by manufacturing TiO_2 materials with a large surface area. TiO_2 gives high acid strength when reacted with sulfuric acid and as a result, $TiSO_4$ is produced. It gives better performance as a heat conductor due to its photocatalytic nature and hence, is useful as a coolant agent. Furthermore, nanofluid becomes more stable with TiO_2 nanoparticles and is useful in motor vehicles to reduce the air population as well. A significant study for energy production in the photocatalysis field is given in [3].

Ternary hybrid nanofluid with three different nanomaterials is an advanced category of liquid that possesses great thermal performance at energy transport when compared with normal liquids. With its unique properties, higher thermal performance, and heat rate enhancement in dynamics of fuel as well as automobile coolants, cumulative knowledge of dual particle nano liquid can be outlined. Moreover, due to its advanced thermal performance it can be used as a coolant agent in radiators and to improve the flow of heat transport. Some applications are magnetic resonance imaging, drug delivery and cancer removal. Saleem et al. [4] analyzed the thermal analysis of cilia transport of blood flow with dispersion of three different nanomaterials in the presence of Lorentz force. Arif et al. [5] discussed the fractional model flow of water with heat transport using three different shaped nanomaterials in the radiator. Das et al. [6] investigated the impact of an electrical double layer on mixed convective flow with three different nanomaterials in a vertical channel in the presence of Lorentz force. Munawar et al. [7] presented a model for hydromagnetic cilia transport of tri-hybrid nano liquid within an elastic electroosmotic pump with mixed convection phenomenon. Ramesh et al. [8] investigated the behavior of base fluid due to the dispersion of three different nanomaterials in a stretchable channel with heat source and sink phenomena. Some latest studies on THNF flow are listed as [9-12].

The heat source and sink phenomena occur due to the difference between the liquid present in the surroundings and the interface. The heat source phenomenon affects the thermal transport in the liquid, and it depends on the heat and space. Some applications are aeration, reactor quality assurance, food manufacturing, combustion analysis, and dilatation. Rajkumar et al. [13] investigated the system disorder due to pulsating hydromagnetic micropolar nano liquid flow in the presence of the Cattaneo-Christov heat flux model and heat source as well as heat sink phenomena in a channel with spongy media. Shobha et al. [14] discussed the micropolar nano liquid in the presence of heat source as well as heat sink phenomena and inclined Lorentz force between vertical plates. Bhaskar et al. [15] discussed the heat source as well as heat sink phenomena with cross-diffusion effects of hydromagnetic nano-liquid flow within a channel in the presence of a chemical reaction. Shobha et al. [16] analyzed the impact of heat source and sink phenomena in Williamson nano-liquid flow with nonlinear thermal radiation within a vertical channel. Jha et al. [17] scrutinized the effect of heat sink and source phenomena on free convection flow through an upright channel having suction and injection phenomena.

The Hall current becomes too important to ignore when magnetic forces increase in magnitude. Hall current is a phenomenon that characterizes the behaviour of electrons in a

conductor when they are being acted upon by electric and magnetic fields. Through a second-law analysis, Roja and Gireesha [18] investigated the Hall effect of natural convection flow in a vertical channel with a constant heat source and sink. In a mixed-convection flow driven by a shifting magnetic flux, effects of Ion slip and Hall currents, thermal radiative heat, and chemical reaction on a viscoelastic fluid flowing down a vertical permeable channel were investigated by Singh et al. [19]. The influence of the generated magnetic field and Hall current on the flow of convective viscoelastic fluid streaming down an upright channel was addressed by Singh et al. [20]. Using Hall current and an induced magnetic field, Singh and Seth [21] analysed the MHD convective flow of a second-grade liquid through two alternately vertical surfaces. The Hall current's impact on the movement of ionised ethylene-glycol in a vertical permeable channel with metal nanoparticles was investigated by Das et al. [22]. Maraj et al. [23] studied the rotating flow of an MHD (MoS_2-SiO_2-H_2O) HNF in a channel due to thermal periodic conditions and velocity slip at its vertical wall.

Motivated by the above-mentioned literature, the current study explores the effects of Hall current on the flow of tri-hybridized nanofluid with two different base liquids and TiO_2, *MWCNTs* and *SWCNTs* as nanoparticles. The liquids are heat absorbing and heat generating and flow through upright vertical plates under the influence of the optically thin limit of thermal radiation. Exact solutions for velocities and temperature profiles are obtained and presented through graphs and tables. Table 1 displays the uniqueness and research gap of the present study.

The present study enhances the existing body of literature by addressing the following research inquiries.

- What effect does the addition of three distinct nanoparticle types have on the heat transfer properties?
- For ternary hybrid nanofluids, what role does Hall current play?
- How might the fluid's temperature be affected by the heat source or sink?

Table 1 Research gap of the study

Ref. No.	[24]	[25]	[26]	Present
Hall current	×	×	✓	✓
Ternary HNF	×	×	×	✓
Heat source/sink	×	×	×	✓
Beavers and Joseph velocity slip	×	✓	✓	✓

2. Mathematical Development of the Problem

In a permeable media saturated with an incompressible tri-hybridized nanofluid, laminar flow affected by a radiative heat flux is investigated. The flow is confined to two vertical porous walls kept along the X-axis to study the effect of suction/injection (Fig. 1). Three types of nanoparticles are considered namely TiO_2, *MWCNTs* and *SWCNTs* in the base fluid water. The two walls are electrically insulated and kept at $Y=0$ and $Y=a$ with temperatures T_0 and T_1 respectively with $T_1>T_0$. The slip is also considered at the cold wall with the suction while the injection is considered at the heated wall. Boussinesq's widely

recognized approximation simplifies the analysis by assuming that all fluid parameters remain constant, except for the density fluctuation with temperature in the body force part.

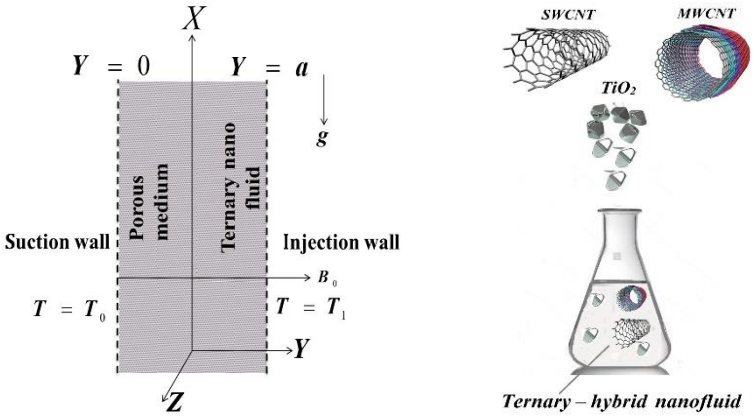

Fig. 1 Schematic of the flow problem

Furthermore, when considering the equations for momentum and energy, density fluctuations have a negligible impact. The temperature differences that are associated with the expansion coefficient are presumed to be the same. The flow is affected by an evenly distributed magnetic field B_0 applied in the Y-direction. Given that Re is so small, the induced magnetic field is negligible. The flow is also governed by Hall effects which raise the Z-component for the velocity. With these assumptions, under the usual Boussinesq approximation, the flow equations for the optically thin fluid subject to thermal radiation with heat source and sink are [25-27]:

$$\partial_{t'}u - v_0\partial_Y u = -\frac{1}{\rho_{thnf}}\partial_X p + \frac{\mu_{thnf}}{\rho_{thnf}}\partial_{YY}u - \frac{\mu_{thnf}}{\rho_{thnf}\,K}u - \frac{\sigma_{thnf}B_0^2\left(u+mw\right)}{\rho_{thnf}\left(1+m^2\right)} + g^*\beta_{thnf}\left(T-T_0\right), \quad (1)$$

$$\partial_{t'}w - v_0\partial_Y w = \frac{\mu_{thnf}}{\rho_{thnf}}\partial_{YY}w - \frac{\mu_{thnf}}{\rho_{thnf}\,K}w - \frac{\sigma_{thnf}B_0^2}{\rho_{thnf}\left(1+m^2\right)}\left(w-mu\right), \quad (2)$$

$$\partial_{t'}T - v_0\partial_Y T = \frac{\mu_{thnf}}{\rho_{thnf}}\frac{k_{thnf}}{\left(\rho C_p\right)_{thnf}}\partial_{YY}T + \frac{4\alpha^{*2}}{\left(\rho C_p\right)_{thnf}}\left(T-T_0\right) + \frac{Q^*}{\left(\rho C_p\right)_{thnf}}\left(T-T_0\right), \quad (3)$$

with the boundary constraints

$$\begin{aligned} &u\big|_{Y=0} = \frac{\sqrt{K}}{\alpha}\partial_Y u\big|_{Y=0}, \quad w\big|_{Y=0} = \frac{\sqrt{K}}{\alpha}\partial_Y w\big|_{Y=0}, \; T\big|_{Y=0} = T_0, \\ &u\big|_{Y=a} = 0, \qquad w\big|_{Y=a} = 0, \qquad T\big|_{Y=a} = T_1. \end{aligned} \quad (4)$$

where t' represents time, u and w are velocity components in X and Z directions, v_0 *is* uniform horizontal velocity, p is the pressure of the fluid, K is the permeability of porous

media, B_0 is magnetic flux strength, m is Hall current parameter, g is gravitational acceleration, Q^* is a heat source, $\boldsymbol{\alpha}^*$ is mean radiative absorption coefficient, T is the fluid temperature, T_0 is the temperature of reference, $\boldsymbol{\alpha}$ is the dimensionless quantity depending on the material, a is the distance between the plates, $\boldsymbol{\rho}_{thnf}$, $\boldsymbol{\mu}_{thnf}$, $\boldsymbol{\beta}_{thnf}$, $(C_p)_{thnf}$, k_{thnf}, $\boldsymbol{\sigma}_{thnf}$ are density, viscosity, thermal expansion, heat capacitance, thermal conductivity and electrical conductivity of THNF, respectively. Derivatives regarding X, Y and t' are indicated by the corresponding subscripts X, Y and t', respectively.

The thermophysical properties of THNF are given as follows [7, 27] whereas the numerical values of these properties are given in Table 2.

$$\frac{\boldsymbol{\rho}_{thnf}}{\boldsymbol{\rho}_f}=\left(1-\boldsymbol{\phi}_1\right)\left(\left(1-\boldsymbol{\phi}_2\right)\left(1-\boldsymbol{\phi}_3+\left(\boldsymbol{\phi}_3\right)\frac{\boldsymbol{\rho}_3}{\boldsymbol{\rho}_f}\right)+\left(\boldsymbol{\phi}_2\right)\frac{\boldsymbol{\rho}_2}{\boldsymbol{\rho}_f}\right)+\left(\boldsymbol{\phi}_1\right)\frac{\boldsymbol{\rho}_1}{\boldsymbol{\rho}_f},\ \frac{\boldsymbol{\mu}_{thnf}}{\boldsymbol{\mu}_f}=\frac{\left(1-\boldsymbol{\phi}_1\right)^{-2.5}}{\left(1-\boldsymbol{\phi}_2\right)^{2.5}\left(1-\boldsymbol{\phi}_3\right)^{2.5}},$$

$$\frac{\left(\boldsymbol{\rho}C_p\right)_{thnf}}{\left(\boldsymbol{\rho}C_p\right)_f}=\left(1-\boldsymbol{\phi}_1\right)\left(\left(1-\boldsymbol{\phi}_2\right)\left(1-\boldsymbol{\phi}_3+\boldsymbol{\phi}_3\frac{\left(\boldsymbol{\rho}C_p\right)_3}{\left(\boldsymbol{\rho}C_p\right)_f}\right)+\boldsymbol{\phi}_2\frac{\left(\boldsymbol{\rho}C_p\right)_2}{\left(\boldsymbol{\rho}C_p\right)_f}\right)+\boldsymbol{\phi}_1\frac{\left(\boldsymbol{\rho}C_p\right)_1}{\left(\boldsymbol{\rho}C_p\right)_f},$$

$$\frac{\boldsymbol{\beta}_{thnf}}{\boldsymbol{\beta}_f}=\left(1-\boldsymbol{\phi}_1\right)\left(\left(1-\boldsymbol{\phi}_2\right)\left(1-\boldsymbol{\phi}_3+\left(\boldsymbol{\phi}_3\right)\frac{\boldsymbol{\beta}_3}{\boldsymbol{\beta}_f}\right)+\left(\boldsymbol{\phi}_2\right)\frac{\boldsymbol{\beta}_2}{\boldsymbol{\beta}_f}\right)+\left(\boldsymbol{\phi}_1\right)\frac{\boldsymbol{\beta}_1}{\boldsymbol{\beta}_f},$$

$$\frac{k_{thnf}}{k_{hnf}}=\frac{k_1+2k_{hnf}-2\left(k_{hnf}-k_1\right)\boldsymbol{\phi}_1}{k_1+2k_{hnf}+\left(k_{hnf}-k_1\right)\boldsymbol{\phi}_1},\quad \text{where}\ \frac{k_{hnf}}{k_{nf}}=\frac{k_2+2k_{nf}-2\left(k_{nf}-k_2\right)\boldsymbol{\phi}_2}{k_2+2k_{nf}+\left(k_{nf}-k_2\right)\boldsymbol{\phi}_2},\qquad (5)$$

$$\frac{k_{nf}}{k_f}=\frac{k_3+2k_f-2\left(k_f-k_3\right)\boldsymbol{\phi}_3}{k_3+2k_f+\left(k_f-k_3\right)\boldsymbol{\phi}_3},\qquad \frac{\boldsymbol{\sigma}_{thnf}}{\boldsymbol{\sigma}_{hnf}}=\frac{\boldsymbol{\sigma}_1+2\boldsymbol{\sigma}_{hnf}-2\boldsymbol{\phi}_1\left(\boldsymbol{\sigma}_{hnf}-\boldsymbol{\sigma}_1\right)}{\boldsymbol{\sigma}_1+2\boldsymbol{\sigma}_{hnf}+\left(\boldsymbol{\sigma}_{hnf}-\boldsymbol{\sigma}_1\right)\boldsymbol{\phi}_1},$$

$$\text{where}\ \frac{\boldsymbol{\sigma}_{hnf}}{\boldsymbol{\sigma}_{nf}}=\frac{\boldsymbol{\sigma}_2+2\boldsymbol{\sigma}_{nf}-2\boldsymbol{\phi}_2\left(\boldsymbol{\sigma}_{nf}-\boldsymbol{\sigma}_2\right)}{\boldsymbol{\sigma}_2+2\boldsymbol{\sigma}_{nf}+\left(\boldsymbol{\sigma}_{nf}-\boldsymbol{\sigma}_2\right)\boldsymbol{\phi}_2},\qquad \frac{\boldsymbol{\sigma}_{nf}}{\boldsymbol{\sigma}_f}=\frac{\boldsymbol{\sigma}_1+2\boldsymbol{\sigma}_f-2\boldsymbol{\phi}_1\left(\boldsymbol{\sigma}_f-\boldsymbol{\sigma}_1\right)}{\boldsymbol{\sigma}_1+2\boldsymbol{\sigma}_f+\left(\boldsymbol{\sigma}_f-\boldsymbol{\sigma}_1\right)\boldsymbol{\phi}_1}.$$

In the above expressions, the term $\boldsymbol{\phi}_{1,2,3}$ relates to volume fraction for nanoparticles. Hybrid nanofluid, nanofluid, and fluid are indicated by the subscripts *hnf*, *nf*, and *f* respectively.

Table 2 Numerical values for physical properties of nanoparticles and base fluids [7, 28, 29]

Properties	H_2O	*Kerosene*	TiO_2	*SWCNTs*	*MWCNTs*
$\boldsymbol{\rho}$ (Kg/m^3)	997	783	4250	2600	1600
k $(Wm^{-1}K^{-1})$	0.613	0.145	8.9583	6600	3000
C_p $(Jkg^{-1}K^{-1})$	4179	2090	686.2	425	796
$\boldsymbol{\sigma}$ (S/m)	0.05	$6*10^{-10}$	$1*10^{-12}$	1400	300
$\boldsymbol{\beta}$ (K^{-1})	$21*10^{-5}$	$99*10^{-5}$	$0.9*10^{-5}$	$19*10^{-6}$	$21*10^{-6}$
Pr	6.2	27.6	--	--	--

To reduce the system to a dimensionally independent form, the following non-dimensional quantities are used forthcoming non-dimensional quantities are used.

$$
\begin{aligned}
&y=\frac{X}{a},\quad y=\frac{Y}{a},\quad f=\frac{u\,a}{\upsilon_f},\quad g=\frac{w\,a}{\upsilon_f},\quad \theta=\frac{T-T_0}{T_1-T_0},\quad t=\frac{t'\upsilon_f}{a^2},\\
&\mathrm{P}=\frac{a^2\,p}{\upsilon_f^2\,\rho_f},\quad \mathrm{Gr}=\frac{g^*\beta_f\,(T_1-T_0)a^3}{\upsilon_f^2},\quad \gamma=\frac{\sqrt{K}}{\alpha\,a},\quad Da=\frac{K}{a^2},\quad s=\frac{v_0 a}{\upsilon_f},\\
&Ha^2=\frac{a^2\sigma_f\,B_0^2}{\upsilon_f\,\rho_f},\quad \mathrm{Pr}=\frac{\upsilon_f\left(\rho C_p\right)_f}{k_f},\quad \delta=\frac{4\alpha^{*2}a^2}{(\rho Cp)_f\,\upsilon_f},\quad Q=\frac{Q^*a^2}{k_f}.
\end{aligned}
\tag{6}
$$

Together, the surface constraints and the flow equations can be expressed as

$$
\partial_t f - s\partial_y f = -\frac{1}{\rho}\partial_x P+\frac{\mu^*}{\rho^*}\partial_{yy} f-\frac{\mu^*}{\rho^*}\frac{1}{Da}\,f+\beta^* Gr\theta-\frac{\sigma^*}{\rho^*}\frac{Ha^2}{1+m^2}\left(f+mg\right),
\tag{7}
$$

$$
\partial_t g - s\partial_y g = \frac{\mu^*}{\rho^*}\partial_{yy} g-\frac{\mu^*}{\rho^*}\frac{1}{Da}\,g-\frac{\sigma^*}{\rho^*}\frac{Ha^2}{1+m^2}\left(g-mf\right),
\tag{8}
$$

$$
\mathrm{Pr}\left(\rho C_p\right)^*\left(\partial_t\theta-s\partial_y\theta\right)=k^*\partial_{yy}\theta+\delta\theta+Q\theta,
\tag{9}
$$

with the surface constraints defined in the following manner:

$$
\begin{gathered}
f\big|_{y=0}=\gamma\,\partial_y f\big|_{y=0},\quad g\big|_{y=0}=\gamma\,\partial_y g\big|_{y=0},\quad \theta\big|_{y=0}=0,\\
f\big|_{y=1}=0,\qquad g\big|_{y=1}=0,\qquad \theta\big|_{y=1}=1.
\end{gathered}
\tag{10}
$$

The parameters in the above expressions are Hartmann number *Ha*, viscosity ratio $\boldsymbol{\mu}^*$, density ratio $\boldsymbol{\rho}^*$, electrical conductivity ratio $\boldsymbol{\sigma}^*$, thermal expansion ratio $\boldsymbol{\beta}^*$, Hall parameter *m*, Garshof number *Gr*, electrical conductivity ratio k^*, Darcy parameter *Da*, suction parameter *s*, Prandtl number Pr, radiation parameter $\boldsymbol{\delta}$, heat source/sink parameter *Q* and slip parameter $\boldsymbol{\gamma}$.

3. METHOD OF SOLUTION

Using $\psi = f + ig$ the system of Eqs. (7-10) can be written as

$$
\partial_t\psi-s\partial_y\psi=-\frac{1}{\rho^*}\partial_x P+\frac{\mu^*}{\rho^*}\partial_{yy}\psi-\frac{\mu^*}{\rho^*}\frac{1}{Da}\psi+\beta^* Gr\theta-\frac{\sigma^*}{\rho^*}\frac{Ha^2}{1+m^2}\left(\psi-i\,m\,\psi\right),
\tag{11}
$$

$$
\mathrm{Pr}\left(\rho C_p\right)^*\left(\partial_t\theta-s\partial_y\theta\right)=k^*\partial_{yy}\theta+\delta\theta+Q\theta,
\tag{12}
$$

and

$$\begin{aligned} \psi\big|_{y=0} &= \gamma\, \partial_y \psi\big|_{y=0}, \quad & \theta\big|_{y=0} &= 0, \\ \psi\big|_{y=1} &= 0, & \theta\big|_{y=1} &= 1. \end{aligned} \tag{13}$$

When dealing with the pure oscillatory flow, the solutions to Eqs. (11)-(13) are obtained by letting [25]

$$-\partial_x P = \lambda e^{i\omega t}, \qquad \psi(y,t) = \psi_0(y) e^{i\omega t}, \quad \theta(y,t) = \theta_0(y) e^{i\omega t}. \tag{14}$$

where λ represents any positive constant and ω is oscillation frequency.

Using Eq. (14) into Eqs. (11-13) give

$$\frac{\mu^*}{\rho^*} D_{yy}\psi_0 + sD_y\psi_0 - q_5\,\psi_0 = -\frac{\lambda}{\rho^*} - \beta^* Gr\theta_0, \tag{15}$$

$$k^*\, D_{yy}\theta_0 + q_1\, D_y\theta_0 + q_2\,\theta_0 = 0, \tag{16}$$

with

$$\begin{aligned} \psi_0\big|_{y=0} &= \gamma\, D_y\psi_0\big|_{y=0}, \quad & \theta_0\big|_{y=0} &= 0, \\ \psi_0\big|_{y=1} &= 0, & \theta_0\big|_{y=1} &= 1. \end{aligned} \tag{17}$$

The fluid temperature expression is produced by solving Eq. (16) with restrictions (17), which leads

$$\theta(y,t) = e^{i\omega t}\left(C_1 e^{q_3 y} + C_2 e^{q_4 y}\right), \tag{18}$$

After solving Eq. (15) under the constraints (17), the expression for the primary and secondary velocities of the fluid are

$$f(y,t) = \mathrm{Cos}(\omega t)\left(C_3 e^{q_6 y} + C_4 e^{q_7 y} + \frac{\lambda}{\rho^* q_5} + q_8 e^{q_3 y} + q_9 e^{q_4 y}\right), \tag{19}$$

$$g(y,t) = \mathrm{Sin}(\omega t)\left(C_3 e^{q_6 y} + C_4 e^{q_7 y} + \frac{\lambda}{\rho^* q_5} + q_8 e^{q_3 y} + q_9 e^{q_4 y}\right). \tag{20}$$

At the left wall (y=0) of the channel, the non-dimensional expressions for shear stresses caused by main and secondary flows are represented by

$$Cf_x + i\,Cf_z = \left.\frac{\partial\psi}{\partial y}\right|_{y=0} = e^{i\omega t}\left(C_3 e^{q_6 y} + C_4 e^{q_7 y} + \frac{\lambda}{\rho^* q_5} + q_8 e^{q_3 y} + q_9 e^{q_4 y}\right), \tag{21}$$

and the rate of heat transfer is given as

$$Nu = \left.\frac{\partial\theta}{\partial y}\right|_{y=0} = e^{i\omega t}\left(C_1 e^{q_3 y} + C_2 e^{q_4 y}\right). \tag{22}$$

The following are the values used in the aforementioned expressions as constants.

$$\rho^* = \frac{\rho_{thnf}}{\rho_f},\ \mu^* = \frac{\mu_{thnf}}{\mu_f},\ \sigma^* = \frac{\sigma_{thnf}}{\sigma_f},\ k^* = \frac{k_{thnf}}{k_f},\ \beta^* = \frac{\beta_{thnf}}{\beta_f},\ \left(\rho C_p\right)^* = \frac{\left(\rho C_p\right)_{thnf}}{\left(\rho C_p\right)_f},\ q_1 = s\,\mathrm{Pr}\left(\rho C_p\right)^*,$$

$$q_2 = \left(\delta + Q - i\,\omega\left(\rho C_p\right)^*\right)\mathrm{Pr},\ q_3 = \frac{1}{2}\left(-\frac{q_1}{k^*} - \frac{\sqrt{q_1^2 - 4k^* q_2}}{k^*}\right),\ q_4 = \frac{1}{2}\left(-\frac{q_1}{k^*} + \frac{\sqrt{q_1^2 - 4k^* q_2}}{k^*}\right),$$

$$q_5 = \frac{\mu^*}{\rho^* Da} + \frac{\sigma^* Ha^2}{\rho^*\left(1+m^2\right)}\left(1 - m\,i\right) + \mathrm{i}\omega, \qquad q_6 = \frac{1}{2}\left(-\frac{s\rho^*}{\mu^*} - \frac{\sqrt{\rho^*}\sqrt{4q_5\mu^* + s^2\rho^*}}{\mu^*}\right),$$

$$q_7 = \frac{1}{2}\left(-\frac{s\rho^*}{\mu^*} + \frac{\sqrt{\rho^*}\sqrt{4q_5\mu^* + s^2\rho^*}}{\mu^*}\right),\ q_8 = -\frac{C_1 Gr\beta^*\rho^*}{q_3^2\mu^* - q_5\rho^* + q_3 s\rho^*},\ q_9 = -\frac{C_2 Gr\beta^*\rho^*}{q_4^2\mu^* - q_5\rho^* + q_4 s\rho^*},$$

$$q_{10} = q_8 + q_9 - \begin{pmatrix} q_3 q_8 \\ +q_4 q_9 \end{pmatrix}\gamma + \frac{\lambda}{q_5\rho^*},\ q_{11} = 1 - \left(q_6\right)\gamma,\quad q_{12} = 1 - \left(q_7\right)\gamma,\ q_{13} = e^{q_3} q_8 + e^{q_4} q_9 + \frac{\lambda}{q_5\rho^*},$$

$$C_1 = \frac{1}{e^{q_3} - e^{q_4}},\quad C_2 = -\frac{1}{e^{q_3} - e^{q_4}},\ C_3 = -\frac{e^{q_7} q_{10} - q_{12} q_{13}}{e^{q_7} q_{11} - e^{q_6} q_{12}},\ C_4 = -\frac{e^{q_6} q_{10} - q_{11} q_{13}}{-e^{q_7} q_{11} + e^{q_6} q_{12}}.$$

4. RESULTS AND DISCUSSION

Hall effects on the flow of tri-hybridized nanofluid with two different base fluids flowing through vertical parallel plates have been discussed. The fluid temperature expression is produced by solving Eqs. (16) with restrictions (17), while after solving Eq. (15) under constraints (17), the expressions for the primary and secondary velocities of the fluid are obtained. During the investigation, the following range of parameters is kept in mind: $0 < \phi_1=\phi_2=\phi_3 \leq 0.06$ (nanoparticles volume fraction), $2 < Ha \leq 3.5$ (Hartman number), $2 < m \leq 3.5$ (Hall parameters), $0 < \delta \leq 1.5$ (radiation parameter), and $-1.5 < Q \leq 1.5$ (Heat source/sink parameter) are used. The values for the other parameters are Da=1, s=1, γ=0.1, and Gr=1.

Fig. 2a shows that the primary flow velocity is higher in the case of pure fluid, but it decreases with the addition of nanoparticles. The velocity is lowest in the case of ternary nanoparticles. As the concentration of nanomaterials in liquids increases, the liquids thicken, and the flow rates decrease. Therefore, primary velocities decrease. The flow velocity is also less for kerosene-based fluid in the case of heat source and an opposite behaviour is observed for the heat sink case (see Fig. 2b). The same behaviour is observed for the secondary flow velocity as can be seen in Figures 2c and 2d. In comparison to pure, hybrid, and mono fluids, the ternary hybrid nanofluid has a lower temperature in both scenarios including base liquids. When the number of nanomaterials added to liquids increases, the liquids thicken significantly, slowing down the flow and reducing convection. Due to this, the temperatures of the liquids decrease. The temperature for the kerosene-based ternary nanofluid is higher as compared to the water-based ternary nanofluid (see Fig. 2e and 2f).

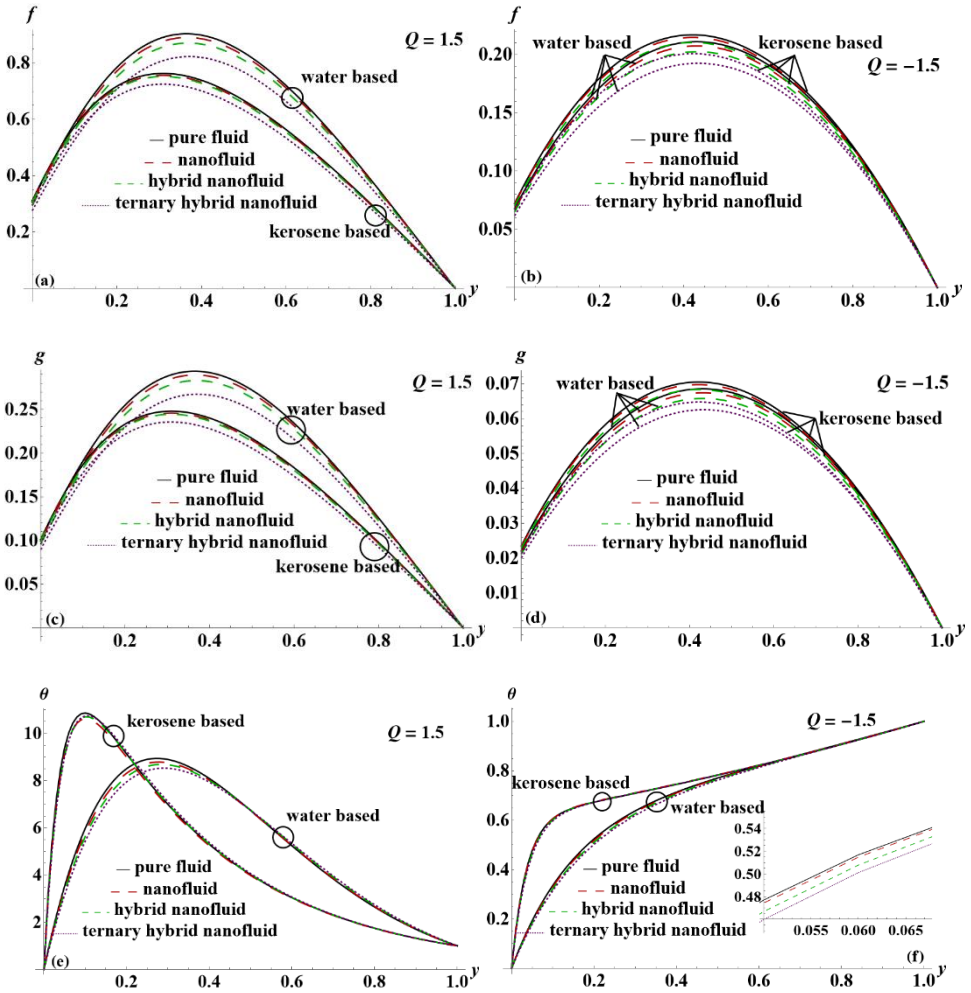

Fig. 2 Comparative analysis with two base fluids (a, b) primary velocity $f(y,t)$ (c, d) secondary velocity $g(y,t)$ and (e, f) temperature $\boldsymbol{\theta}(y,t)$

The effects of the Hartmann number *Ha* on the fluid velocities for THNF are presented in Figure 3. Figures 3a and 3b show the decreasing behaviour of primary fluid velocity with the increasing values of *Ha* for both cases of heat source and sink respectively. Figures 3c and 3d present the decreasing behaviour of secondary velocity with an increase in *Ha* for both cases of heat source and sink respectively. The rise in the resistive Lorentz force, which is associated with the increase in the values of the Hartmann number, is the cause of the decrease in both primary and secondary velocities. The flow velocities are higher for water-based nano liquid as compared to kerosene-based nano liquid.

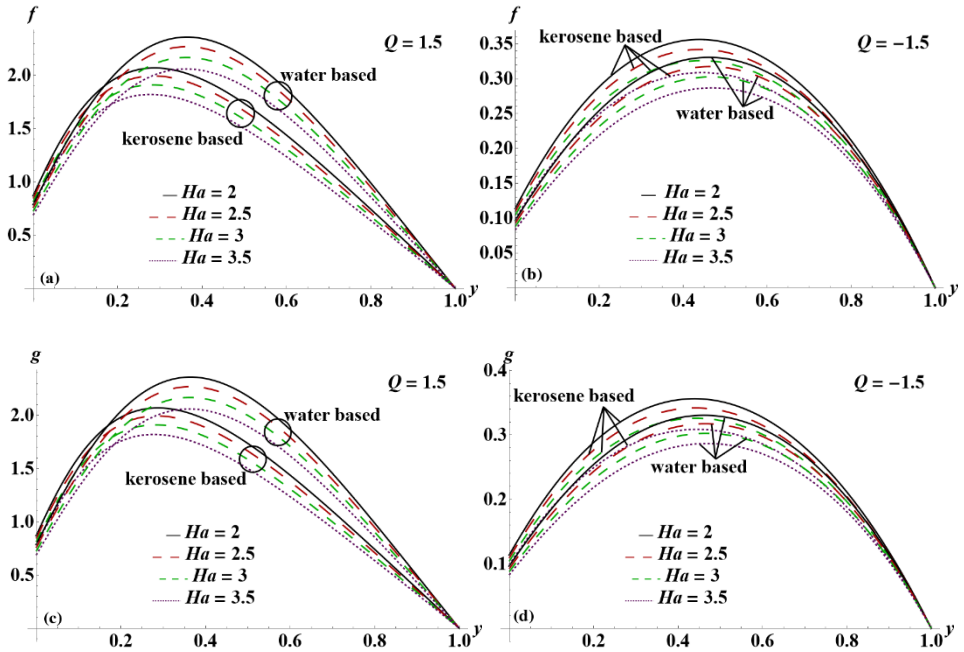

Fig. 3 Variation of (a, b) primary velocity $f(y,t)$ (c, d) secondary velocity $g(y,t)$ against *Ha* for THNF

The effect of Hall parameter *m* on the fluid velocities in the cases of both heat source and heat sink are plotted in Fig. 4. The reverse behaviour is observed in the velocities of THNF with the rise in *m* as compared to *Ha*. When *m* is increased, the effectiveness of conduction decreases, which in turn reduces the magnetic damping and, as a result, enhances the velocity of the fluid. However, the variation in kerosene-based liquid and water-based liquid is like that of *Ha*.

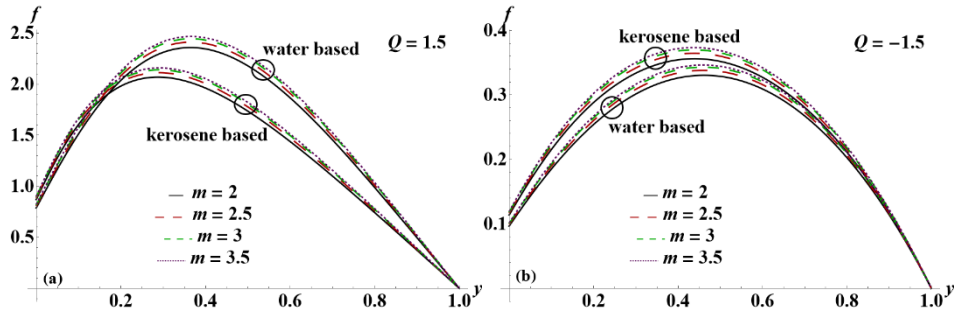

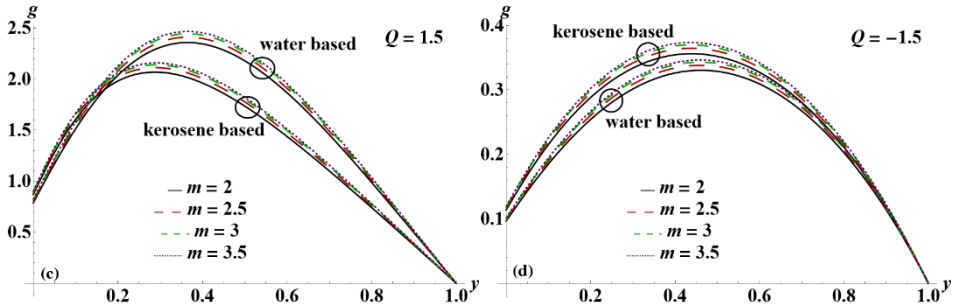

Fig. 4 Variation of (a, b) primary velocity $f(y,t)$ (c, d) secondary velocity $g(y,t)$ against m for THNF

The oscillatory behaviour of both primary and secondary velocities with the increasing values of Ha is shown in Fig. 5. Both the velocities show a decreasing behaviour with escalating values of the Hartmann number for both heat source and heat sink cases. The amplitude for the kerosene-based liquid is higher than water-based liquid

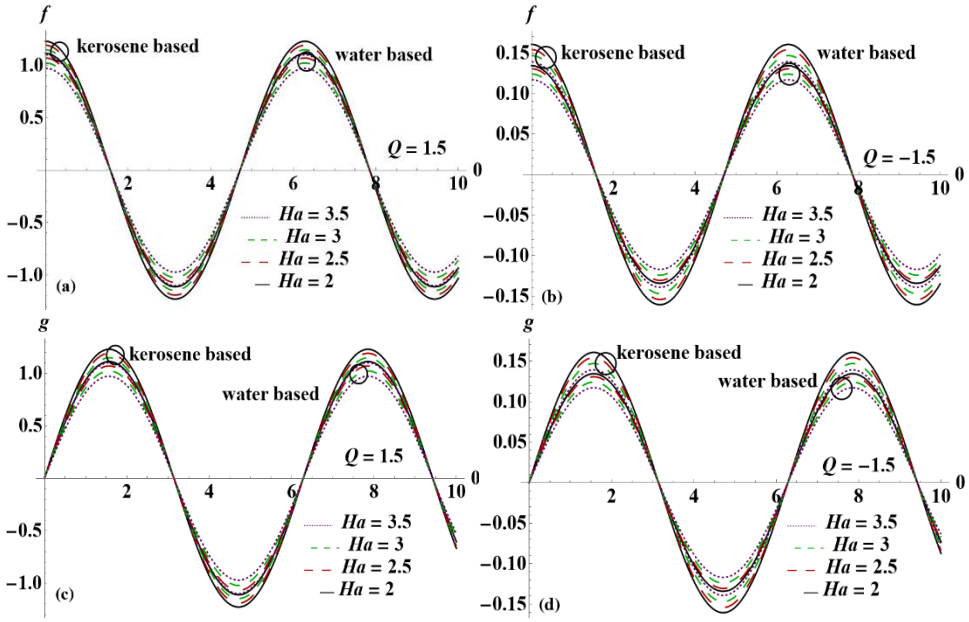

Fig. 5 Oscillatory variation of (a, b) primary velocity $f(y,t)$ (c, d) secondary velocity $g(y,t)$ against Ha for THNF

The oscillatory behaviour of both primary and secondary velocities with the increasing values of m is shown in Fig. 6. Both the velocities show an increasing behaviour with escalating values of the Hall parameter for both heat source and heat sink cases. The amplitude for the kerosene-based liquid is higher than water-based liquid. Also, the amplitude is higher in the case of the heat source relative to the heat sink case.

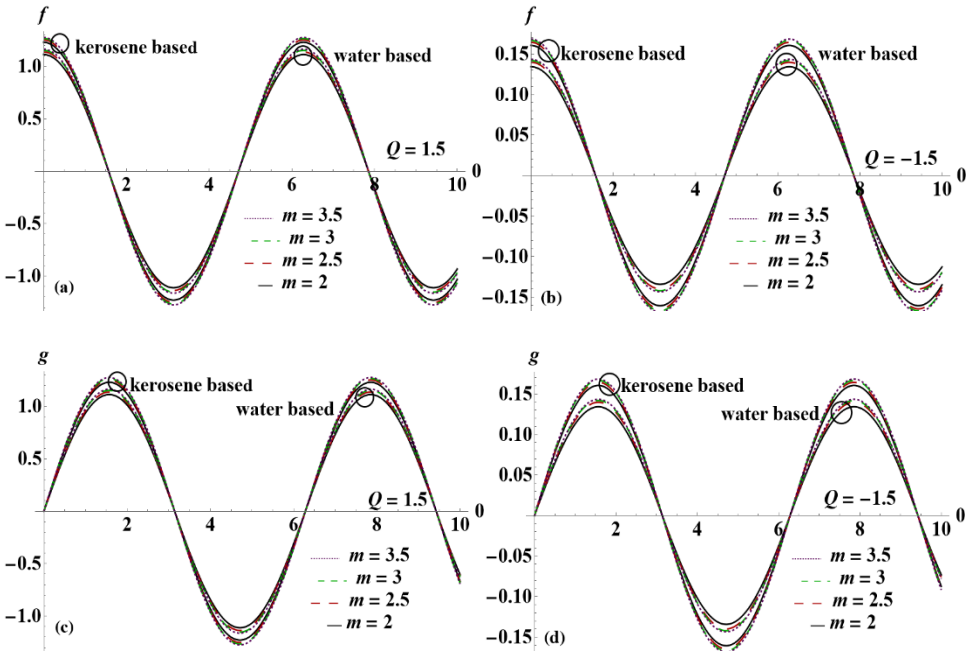

Fig. 6 Oscillatory variation of (a, b) primary velocity $f(y,t)$ (c, d) secondary velocity $g(y,t)$ against m for THNF

The surface frictions due to primary and secondary flow against Ha with the variation in m are presented in Fig. 7. The surface frictions due to both velocities show an increasing behaviour with escalating values of the Hall parameter for both heat source and heat sink cases. However, the opposite behaviour is observed for the increasing values of Ha.

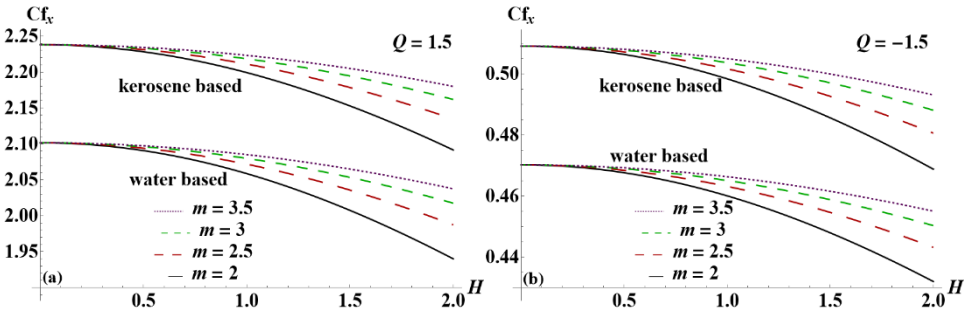

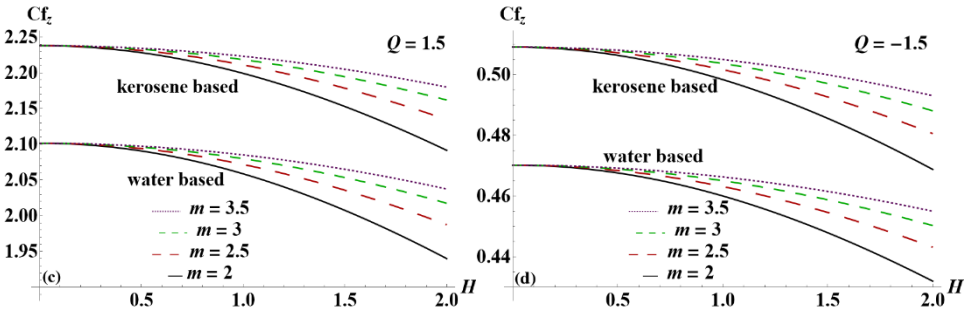

Fig. 7 Variation of surface friction (a, b) Cf_x (c, d) Cf_z

Fig. 8 is plotted to exhibit the heat transfer rate versus radiation parameter with the variation in the volume fraction of nanoparticles in THNF. The heat transmission rate increases with the radiation parameter for both liquids while it reduces with the added nanomaterials. The phenomena are the same for both cases of heat source and heat sink.

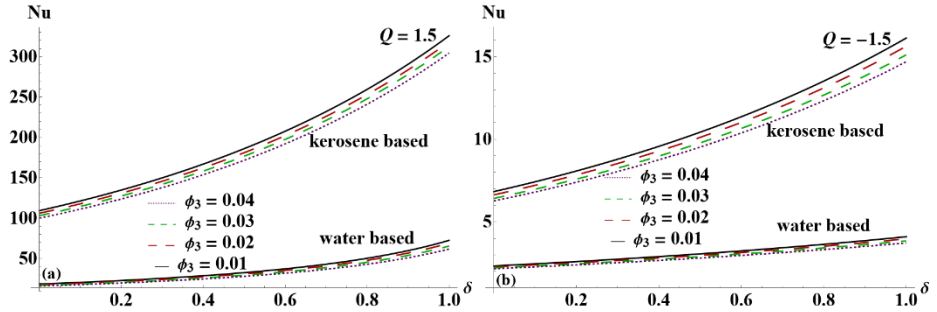

Fig. 8 Variation of heat transfer rate *Nu*

Fig. 9 presents a comparison with the results of the preceding study done by Falade et al. [25]. Both the figures corroborate the earlier findings with values $\phi_1=\phi_2=\phi_3=Q=m=0$.

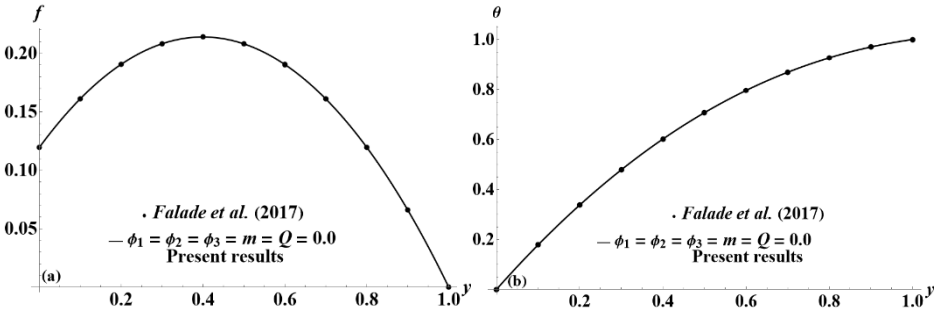

Fig. 9 Comparison of results with the existing literature (a) $f(y,t)$ and (b) $\theta(y,t)$

5. CONCLUSIONS

Hall effects on the flow of tri-hybridized nanofluid with two different base fluids flowing through vertical parallel plates have been discussed. The flow is affected by thermal radiation in the presence of a heat source and sink. The following results have been concluded:

- Primary and secondary flow velocities of the tri-hybridized nanofluid are less than the velocities for the HNFs, NFs and pure base fluids for both the heat source and sink case.
- The velocities for kerosene-based fluids are less than the velocities for the water-based fluids for the heat source case while the opposite behavior is noticed for the heat sink case.
- Both the velocities decrease with an increase in *Ha* for all kinds of kerosene and water-based fluids in both heat source and sink cases. However, the amplitudes for the case of the heat sink are less than the case of the heat source.
- An opposite trend for the velocities is observed for the *m* as compared to *Ha*.
- The temperature for the kerosene-based fluids is greater than for the water-based fluids. However, the temperature of the tri-hybridized nanofluid is less than the temperature for the HNFs, NFs and pure base fluids for both the heat source and sink case.

Even though this study has shed light on the consequences of multi-mass diffusion of nanoparticles in two different base fluids, there are still a great many possible contexts in which this phenomenon could be studied further. For example, this phenomenon could be studied with different combinations of nanoparticles or with different particle shapes. There is also the possibility of doing research into the responses of other common base fluids that are utilized in engineering operations.

REFERENCES

1. De Volder, M.F., Tawfick, S.H., Baughman, R.H., Hart, A.J., 2013, *Carbon nanotubes: present and future commercial applications*, Science, 339(6119), pp. 535-539.
2. Yudasaka, M., Ichihashi, T., Kasuya, D., Kataura, H., Iijima, S., 2003, *Structure changes of single-wall carbon nanotubes and single-wall carbon nanohorns caused by heat treatment*, Carbon, 41(6), pp. 1273-1280.
3. Li, Z., Wang, S., Wu, J., Zhou, W., 2022, *Recent progress in defective TiO2 photocatalysts for energy and environmental applications*, Renew. Sust. Energy Reviews, 156, 111980.
4. Saleem, N., Ashraf, T., Daqqa, I., Munawar, S., Idrees, N., Afzal, F., Afzal, D., 2022, *Thermal case study of cilia actuated transport of radiated blood-based ternary nanofluid under the action of tilted magnetic field*, Coatings, 12(6), 873.
5. Arif, M., Kumam, P., Kumam, W., Mostafa, Z., 2022, *Heat transfer analysis of radiator using different shaped nanoparticles water-based ternary hybrid nanofluid with applications: A fractional model*, Case Stud. Ther. Eng., 31, 101837.
6. Das, S., Ali, A., Jana, R.N., Makinde, O.D., 2022, *EDL impact on mixed magneto-convection in a vertical channel using ternary hybrid nanofluid*, Chem. Eng. J. Advan., 100412.
7. Munawar, S., Saleem, N., 2022. *Mixed convective cilia triggered stream of magneto ternary nanofluid through elastic electroosmotic pump: A comparative entropic analysis*, J. Mol. Liq., 352, 118662.
8. Ramesh, G.K., Madhukesh, J.K., Shehzad, S.A., Rauf, A., 2024, *Ternary nanofluid with heat source/sink and porous medium effects in stretchable convergent/divergent channel.* Proceed. Instit. Mech. Engineers, Part E: J. Process Mech. Eng., 238(1), pp. 134-143.

9. Kumar K.T., Remidi, S., Madhu, J., Kumar, R.N., Gowda, R.J.P., Muhammad, T., Hassan, A.M., Kumar, R., 2024, *The magnetic dipole-induced ternary-hybrid nanofluid flow behavior along a vertical and horizontal wall under free, mixed, and forced convection*, Num. Heat Trans., Part A., Appl., pp. 1-18.
10. Mishra, N.K., Sharma, P., Sharma, B.K., Almohsen, B., Pérez, L.M., 2024, *Electroosmotic MHD ternary hybrid Jeffery nanofluid flow through a ciliated vertical channel with gyrotactic microorganisms: Entropy generation optimization*. Heliyon, 10(3), e25102.
11. Raza, Q., Wang, X., Muhammed, H.A.H., Ali, B., Ali, M.R., Hendy, A.S., 2024, *Numerically analyzed of ternary hybrid nanofluids flow of heat and mass transfer subject to various shapes and size factors in two-dimensional rotating porous channel*, Case Stud. Ther. Eng., 56, 104235.
12. Rehman, A., Abbas, Z., Hussain, Z., Hasnain, J., Mir, A., 2024, *Integration of statistical and simulation analyses for ternary hybrid nanofluid over a moving surface with melting heat transfer*, Nanotechnology, 35(26), 265401.
13. Rajkumar, D., Subramanyam Reddy, A., Chamkha, A.J., 2022, *Entropy generation of magnetohydrodynamic pulsating flow of micropolar nanofluid in a porous channel through Cattaneo–Christov heat flux model with Brownian motion, thermophoresis and heat source/sink*, Waves in Random and Comp. Media, pp. 1-26.
14. Shobha, K.C., Patil, M.B., 2022, *Irreversibility analysis of micropolar nanofluid flow in a vertical channel with the impact of inclined magnetic field and heat source or sink*, Heat Transfer, 51(3), pp. 2723-2741.
15. Bhaskar, K., Sharma, K., Bhaskar, K., 2022, *Cross-diffusion and chemical reaction effects of a MHD nanofluid flow inside a divergent/convergent channel with heat source/sink*, J. Thermal Anal. Calorimetry, pp. 1-16.
16. Shobha, K.C., Patil Mallikarjun, B., 2022, *Effect of Nonlinear Thermal Radiation on Flow of Williamson Nanofluid in a Vertical Porous Channel with Heat Source or Sink by Using Adomian Decomposition Method*, J. Nanofluids, 11(1), pp. 39-47.
17. Jha, B.K., Altine, M.M., Hussaini, A.M., 2022, *Role of Suction/Injection on Free Convective Flow in a Vertical Channel in the Presence of Point/Line Heat Source/Sink*, J. Heat Trans., 144(6), 062602.
18. Roja, A., Gireesha, B.J., 2020, *Second law analysis on Hall effect of natural convection flow through vertical channel in the presence of uniform heat source/sink*, Int. J. Numer. Meth. Heat & Fluid Flow, 30(10), pp. 4403-4423.
19. Singh, J.K., Seth, G.S., Joshi, N., Srinivasa, C.T., 2020, *Mixed convection flow of a viscoelastic fluid through a vertical porous channel influenced by a moving magnetic field with Hall and ion-slip currents, rotation, heat radiation and chemical reaction*, Bulg. Chem. Commun., 52(1), pp. 147-158.
20. Singh, J.K., Seth, G.S., Savanur, V., 2021, *Impacts of the periodic wall conditions on the hydromagnetic convective flow of viscoelastic fluid through a vertical channel with Hall current and induced magnetic field*, Heat Transfer, 50(2), pp. 1812-1835.
21. Singh, J.K., Seth, G.S., 2022, *Scrutiny of convective MHD second-grade fluid flow within two alternatively conducting vertical surfaces with Hall current and induced magnetic field*, Heat Transfer, 51(8), pp. 7613-7634.
22. Das, S., Banu, A.S., Jana, R.N., Makinde, O.D., 2022, *Hall current's impact on ionized ethylene glycol containing metal nanoparticles flowing through vertical permeable channel*, J. Nanofluids, 11(3), pp. 453-467.
23. Maraj, E.N., Zehra, I., Akbar, N.S., 2022, *Rotatory flow of MHD (MoS_2-SiO_2)/H_2O hybrid nanofluid in a vertical channel owing to velocity slip and thermal periodic conditions*, Coll. and Surf. A: Physicochemical Eng. Aspects, 639, 128383.
24. Mehmood, A., Ali, A, 2007, *The effect of slip condition on unsteady MHD oscillatory flow of a viscous fluid in a planer channel*, Roman. J. Phys., 52(1-2), pp. 85-91.
25. Falade, J.A., Ukaegbu, J.C., Egere, A.C., Adesanya, S.O., 2017, *MHD oscillatory flow through a porous channel saturated with porous medium*, Alexand. Eng. J., 56, pp. 147-152.
26. Das, S., Banu, A.S., Jana, R.N., Makinde, O.D., 2022, *Hall current's impact on ionized ethylene glycol containing metal nanoparticles flowing through vertical permeable channel*, J. Nanofluids, 11, pp. 453-467.
27. Hasnain, J., 2024, *Irreversibility analysis for unsteady slip flow of heat absorptive liquid with multiple mass diffusion of nanomaterials over a permeable vertical moving plate: A comparative study*, Proceed. Instit. Mech. Engineers, Part E: J. Process Mech. Eng., https://doi.org/10.1177/09544089241239824
28. Saqib, M., Kasim, A.R.M., Muhammad, N.F., Ching, D.L.C., Shafie, S., 2020, *Application of fractional derivative without singular and local kernel to enhanced heat transfer in CNTs nanofluid over an inclined plate*, Symmetry, 12, 768.

29. Abbas, Z., Rafiq, M.Y., Hasnain, J., Mustafa, G., Arslan, M.S., 2024, *Enhanced thermal study in hybrid nanofluid flow through a channel motivated by water/Cu+Al_2O_3 and entropy generation*, Spectrum of Mechanical Engineering and Operational Research, 1, pp. 131-144.